$$\times \int_0^1 E(\eta)^2 \psi_f' \psi_n \,\mathrm{d}\eta + \int_0^1 F(\xi)^2 \phi_i^n \phi_m \,\mathrm{d}\xi \int_0^1 E(\eta) \psi_j \psi_n^m \,\mathrm{d}\eta$$

$$+ \int_0^1 F(\xi)^2 \phi_i \phi_m^n \,\mathrm{d}\xi \int_0^1 E(\eta) \psi_j^n \psi_n \,\mathrm{d}\eta + 2 \int_0^1 F(\xi) \phi_i' \phi_m \,\mathrm{d}\xi$$

$$\times \int_0^1 E(\eta) \psi_j' \psi_n^m \,\mathrm{d}\eta + 2 \int_0^1 F(\xi) \phi_j \phi_m' \,\mathrm{d}\xi \int_0^1 \psi_j^n \psi_n' \,\mathrm{d}\eta \Bigg]$$

$$+ \nu \left(\frac{c_r}{L}\right)^2 \Bigg[\int_0^1 F(\xi)^2 \phi_j^m \phi_m^n \,\mathrm{d}\xi \int_0^1 E(\eta)^3 \psi_j \psi_n \,\mathrm{d}\eta$$

$$+ 2 \int_0^1 F(\xi) \phi_i' \phi_m^n \,\mathrm{d}\xi \int_0^1 E(\eta)^2 \psi_j' \psi_n \,\mathrm{d}\eta + \int_0^1 \phi_j^n \phi_m \,\mathrm{d}\xi$$

$$\times \int_0^1 E(\eta) \psi_j \psi_n^m \,\mathrm{d}\eta + \int_0^1 F(\xi)^2 \phi_i^m \phi_m^n \,\mathrm{d}\xi \int_0^1 E(\eta)^3 \psi_j \psi_n \,\mathrm{d}\eta$$

$$+ 2 \int_0^1 F(\xi) \phi_i' \phi_m^n \,\mathrm{d}\xi \int_0^1 E(\eta)^2 \psi_j' \psi_n \,\mathrm{d}\eta + \int_0^1 \phi_i \phi_m^n \,\mathrm{d}\xi$$

$$\times \int_0^1 E(\eta) \psi_j^n \psi_n \,\mathrm{d}\eta \Bigg] + 2(1-\nu) \left(\frac{c_r}{L}\right)^2 \Bigg[\int_0^1 F(\xi)^2 \phi_i^n \phi_m^n \,\mathrm{d}\xi$$

$$\times \int_0^1 E(\eta) \psi_j \psi_n \,\mathrm{d}\eta + \int_0^1 \phi_i' \phi_m' \,\mathrm{d}\xi \int_0^1 E(\eta) \psi_j' \psi_n' \,\mathrm{d}\eta$$

$$+ \int_0^1 F(\xi) \phi_i^n \phi_m' \,\mathrm{d}\xi \int_0^1 E(\eta) \psi_j \psi_n' \,\mathrm{d}\eta$$

$$+ \int_0^1 F(\xi) \phi_j' \phi_m^n \,\mathrm{d}\xi \int_0^1 E(\xi)^2 \psi_j' \psi_n \,\mathrm{d}\eta \Bigg] \Bigg\}$$

References

[1]Hopkins, M. A., and Dowell, E. H., "Limited Amplitude Panel Flutter with a Temperature Differential," *Proceeding of the AIAA/ASME/ASCE/AHS/ASC 35th Structures, Structural Dynamics, and Materials Conference*, AIAA, Washington, DC, 1994, pp. 1343–1355.

[2]Weiliang, Y., and Dowell, E. H., "Limit-Cycle Oscillation of a Fluttering Cantilever Plate," *AIAA Journal*, Vol. 32, No. 12, 1994, pp. 2426–2432.

[3]Tang, D. M., Dowell, E. H., and Hall, K. C., "Limit-Cycle Oscillations of a Cantilevered Wing in Low Subsonic Flow," *AIAA Journal*, Vol. 37, No. 3, 1999, pp. 364–371.

[4]Tang, D. M., Henry, J. K., and Dowell, E. H., "Limit-Cycle Oscillations of a Delta Wing Model in Low Subsonic Flow," *AIAA Journal*, Vol. 37, No. 11, 1999, pp. 1355–1362.

[5]Bakhtiari-Nejad, F., and Shokrollahi, S., "Aeroelastic Eigenanalysis of a Cantilever Plate in Low Subsonic Flow to Predict Flutter Onset," *Proceedings of the 10th International Mechanical Engineering Conference*, Iranian Society of Mechanical Engineering (ISME), Tehran, May 2002.

[6]Bakhtiari-Nejad, F., Shokrollahi, S., and Dardel, M., "Effect of Local Forcing Functions on Flutter Suppression of a Low Aspect Ratio Rectangular Cantilever Plate," *Proceedings of the Ninth International Congress on Sound and Vibration*, Orlando, FL, July 2002.

[7]Meirovitch, L., *Principles and Techniques of Vibrations*, Prentice–Hall International Inc., 1997, pp. 522–531.

[8]Dowell, E. H., *Aeroelasticity of Plates and Shells*, Noordhoff International Publ., Leyden, The Netherlands, 1975, pp. 35–49.

[9]Doggett, R. V., and Soistman, D. L., "Some Low-Speed Flutter Characteristics of Simple Low-Aspect-Ratio Delta Wing Models," NASA TM-101547, Jan. 1989.

High-Order Compact Difference Scheme Applied to Double-Delta Wing Vortical Flows

Tomoyuki Arasawa*
Yokohama National University, Kanagawa 240-8501, Japan
Kozo Fujii†
Japan Aerospace Exploration Agency, Kanagawa 229-8510, Japan
and
Koji Miyaji‡
Yokohama National University, Kanagawa 240-8501, Japan

I. Introduction

DELTA wings are suitable for modern high-speed aircrafts due to the low drag at transonic and supersonic regimes. Indeed, a double-delta wing is especially favored because it has mixed characteristics of simple delta wings with small to large leading-edge swept-back angles. The performances of delta wings at landing or takeoff conditions are unfavorable because they require high angles of attack to attain necessary lifts at low speeds. The characteristics of delta wings for such flow conditions are governed by the leading-edge separation vortices over the wing. A number of investigations have been carried out for simple delta wings. From the viewpoint of numerical simulations, fairly accurate predictions are possible by today's computational fluid dynamics technique for low to moderately high angles of attack, that is, before vortex breakdown or lift stall occurs. On the other hand, there have not been sufficient studies on the flow over a double-delta wing despite their practical importance. Numerical accuracy for the problem has not been validated. Two vortices exist for each side of a double-delta wing; one is originating from the leading edge of the strake and the other from the main wing. These vortices interact with each other and eventually merge downstream. Thus, the flows over a double-delta wing are more complex than over a simple delta wing. In our previous effort,[1] the effects of grid resolution were examined by using fairly fine grids, but the results were not satisfactory when compared with the experiment,[2] even with the finest grid using 8 million points.

The purpose of this study is to improve the reliability of the numerical simulations of a double-delta wing using a high-order compact difference scheme.[3] It is a family of spatially implicit schemes, a subset of which are the well-known Padé approximations. The scheme is easily extended to higher-order accuracy with a small number of stencils and it has spectrallike resolutions. Its effectiveness have been reported in recent years for computational aeroacoustics, for example, where sound waves with small pressure fluctuations need to be captured accurately. In this paper, as the most standard scheme today, Roe's upwind scheme[4] is also used. The

Presented as Paper 2003-3537 at the AIAA 16th Computatinal Fluid Dynamics Conference, Orlando, FL, 23 June 2003; received 13 July 2003; revision received 4 January 2004; accepted for publication 12 January 2004.

*Graduate Student, Department of Environment and System Sciences, 79-5 Tokiwadai, Hodogaya, Yokohama.

†Professor, Institute of Space and Astronautical Sciences, 3-1-1 Yoshinodai, Sagamihara. Associate Fellow AIAA.

‡Lecturer, Department of Ocean and Space System Engineering, 79-5 Tokiwadai, Hodogaya, Yokohama. Member AIAA.

results using these schemes are compared with the experimental data reported by Brennenstuhl and Hummel.[2]

II. Numerical Method

The governing equations are the three-dimensional Navier–Stokes equations. The Baldwin–Lomax turbulence model with the Degani–Schiff modification is used. The following sixth-order compact difference scheme is used to evaluate the spatial derivatives. For any scalar quantity f, the spatial derivatives are obtained as

$$\alpha\left(\frac{\partial f}{\partial \xi}\right)_{i-1} + \left(\frac{\partial f}{\partial \xi}\right)_{i} + \alpha\left(\frac{\partial f}{\partial \xi}\right)_{i+1} = a\frac{f_{i+1} - f_{i-1}}{2} + b\frac{f_{i+2} - f_{i-2}}{4} \tag{1}$$

with $\alpha = 1/3$, $a = 14/9$, and $b = 1/9$ for a sixth-order scheme. The extension of Eq. (1) to Navier–Stokes equations is straightforward. The same method is applied to all of the spatial derivatives in convective terms, viscous terms, metrics, and Jacobian. The right-hand side of Eq. (1) is known at n time steps, and the spatial derivatives, $\partial f/\partial \xi$, at each i location is obtained by solving the tridiagonal system. Equation (1) has five stencils in the right-hand side and three stencils in the left-hand side, and thus, it cannot be used in areas near the boundaries. A fourth-order, five-point, explicit one-sided finite difference scheme is used for the evaluation of the derivatives at the points on the boundary. Similarly, one-sided biased finite difference is used at the first interior point.[5]

The filtering procedure is an important component of the compact difference scheme to suppress numerical instabilities arising from unresolved scales, mesh nonuniformities, and boundary conditions. The following filtering scheme[6,7] is used at the interior points:

$$\alpha_f \hat{q}_{i-1} + \hat{q}_i + \alpha_f \hat{q}_{i+1} = \sum_{n=0}^{N} \frac{a_n}{2}(q_{i+n} + q_{i-n}) \tag{2}$$

where q is a component of the solution vector and $\hat{\boldsymbol{q}}$ is the filtered value. The sixth-order filter is obtained with

$$a_0 = 11/16 + (5/8)\alpha_f, \qquad a_1 = 15/32 + (17/16)\alpha_f$$

$$a_2 = -3/16 + (3/8)\alpha_f, \qquad a_3 = 1/32 - (1/16)\alpha_f$$

where α_f is a free parameter satisfying the inequality $-0.5 < \alpha_f \leq 0.5$. In this range, a higher value of α_f corresponds to a less dissipative filter. A fourth-order filter is adopted at the first interior point. For multidimensional problems, the described procedure is sequentially applied for each direction.

Roe's flux difference splitting scheme extended to the third-order accuracy by MUSCL[8] interpolation is also used for the comparison. The viscous terms are evaluated by the second-order central difference for the scheme.

Once all of the spatial derivatives are computed at the nth step, the time-integration process is carried out. The same time-integration algorithm is used for both the schemes. An efficient implicit scheme, the four-factored symmetric Gauss–Seidel (see Ref. 9) is used.

III. Results and Discussions

Effect of the Parameter α_f

The effect of the free parameter α_f is investigated by a vortex convection problem before application to the flow over a double-delta wing. The initial vortex conditions are given as

$$v_\theta = \frac{\Gamma}{2\pi r}\frac{r^2}{r^2 + r_{\text{core}}^2}, \qquad \frac{\mathrm{d}p}{\mathrm{d}r} = \frac{\rho v_\theta^2}{r}$$

$$\frac{\gamma p/\rho}{\gamma - 1} + \frac{v_\theta^2}{2} = \frac{\gamma p_\infty/\rho_\infty}{\gamma - 1} \tag{3}$$

where v_θ is the velocity magnitude in the circumferential direction, $\Gamma = 0.9$, and $r_{\text{core}} = 1$. The vortex is conveyed downstream with freestream Mach number of 0.2. Figure 1 shows the time history of the pressure at the vortex core and a comparison of the ideal result, Roe's third-order scheme, and the sixth-order compact difference schemes with $\alpha_f = 0.40$, 0.45, and 0.49. All of the results by the compact scheme are better than those obtained by use of Roe's scheme. The higher values of α_f show improved results. However, the pressure contour plots shown in Fig. 2a for $\alpha_f = 0.40$ and Fig. 2b for $\alpha_f = 0.49$ show small pressure deviations around the vortex. The noises are severer for the case of $\alpha_f = 0.49$, whereas the difference of the pressure at the vortex core after 200-nondimensional time units is 0.2% of the ambient pressure between $\alpha_f = 0.40$ and 0.49. From the viewpoint of the accuracy and the stability, $\alpha_f = 0.40$ is selected in the following computations.

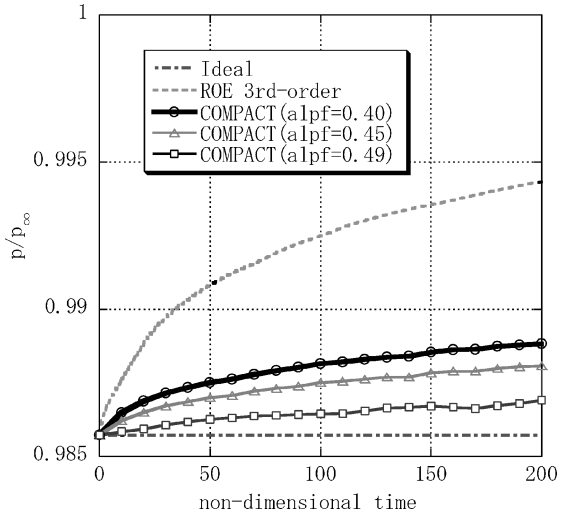

Fig. 1 Time history of the pressure at the vortex core.

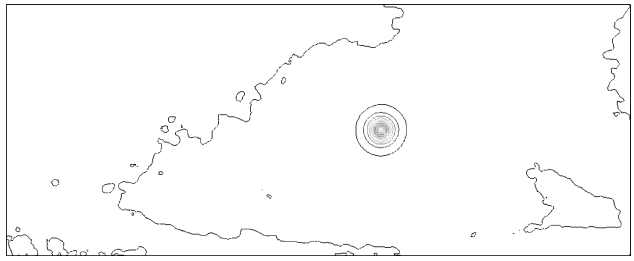

a) $\alpha_f = 0.40$

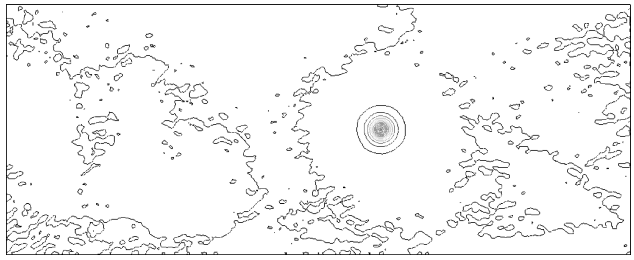

b) $\alpha_f = 0.49$

Fig. 2 Pressure contour plots at 200 nondimensional time: $0.985 \leq p/p_\infty \leq 1.00$.

Double-Delta Wing

The geometry of the double-delta wing is the same as the experimental model used by Brennenstuhl and Hummel.[2] The swept-back angles of the double-delta wing are 80 deg for a strake and 60 deg for a main wing, respectively. The wing has a cylindrically rounded leading edge. Figure 3 shows the computational grid around the wing. The total number of grid points is 810,633.

Flow conditions are listed subsequently. The Reynolds number is 1.3×10^6 based on the root-chord length. Freestream Mach number

is set to 0.3 in this study to simulate the low-speed wind-tunnel experiment. The angles of attack are 12, 13, and 15 deg.

Aerodynamic Coefficients

Figures 4a and 4b show the lift and the pitching moment coefficients, respectively. The pitching moment is positive when the nose is up and the center of the moment is located at N25, which is 59.1% station of the root chord. The length scale for the normalization of the moment is 54.6% root-chord length as in the experiment. The result around 12-deg angle of attack is discussed mainly because precise experimental data are available for the validation. The lift and the pitching moments show good agreement with the experiment by use of both of the schemes, although the pitching moments predicted by the compact difference scheme are slightly larger than the experiment. The reason is discussed by investigating the local flowfields.

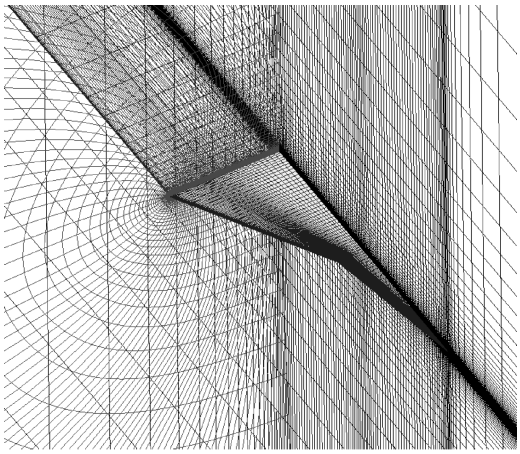

Fig. 3 Computational grid, double-delta wing. ($j \times k \times l = 109 \times 111 \times 67$.)

Local Flowfields

The computed total pressure contour plots at 12-deg angle of attack are shown in Figs. 5a and 5b for the compact difference scheme and Roe's scheme, respectively. Two vortices are observed in both results, one from the strake and the other from the main wing. In addition, a secondary separation vortex is also observed near the leading edge of the main wing. In Fig. 5a, the cores of the two vortices are tighter, and two distinct vortices exist downstream compared with the results in Fig. 5b. When Roe's scheme is used, the vortices are diffused, and they begin to merge just behind the kink of the leading edge. Use of the compact difference scheme results in the higher resolutions.

Figures 6a and 6b show the total pressure contour plots at 75% chordwise section for the respective schemes. The contours obtained by the experiment are overlaid for comparison. The position and the strength of the primary vortex from the main wing are well predicted by the compact difference scheme; moreover, the secondary vortex near the leading edge is larger, and the extent is closer to the experiment with the compact difference scheme. As for the vortex from the strake, the position of the vortex core from the experiment is located between the prediction by compact difference scheme and by Roe's scheme. The two vortices are independent, and little interaction is seen in Fig. 6a, whereas too many interactions and vortex merging occur as shown in Fig. 6b. The vortex from the strake is laterally extended due to interaction with use of Roe's scheme. Possible reasons for the discrepancies on the vortex from the stake are the effect of the turbulence model and the flow unsteadiness.

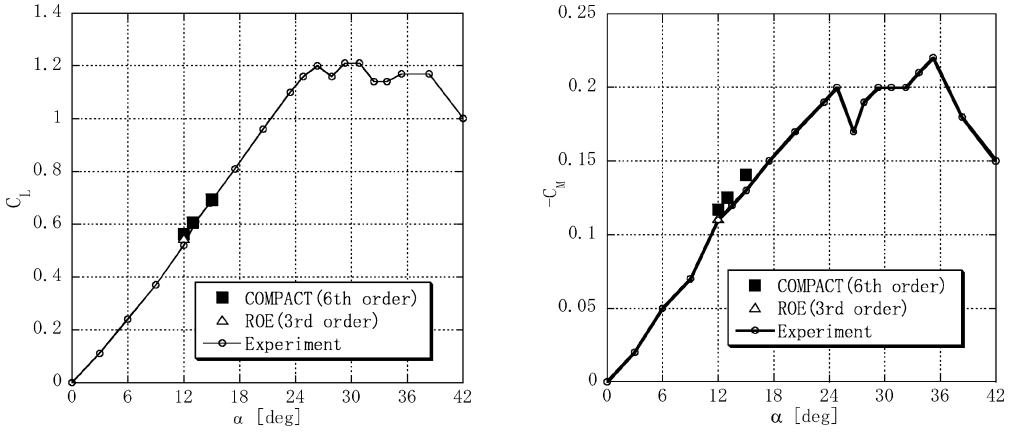

a) Lift coefficient **b) Pitching moment coefficient**

Fig. 4 Aerodynamic coefficients vs angle of attack.

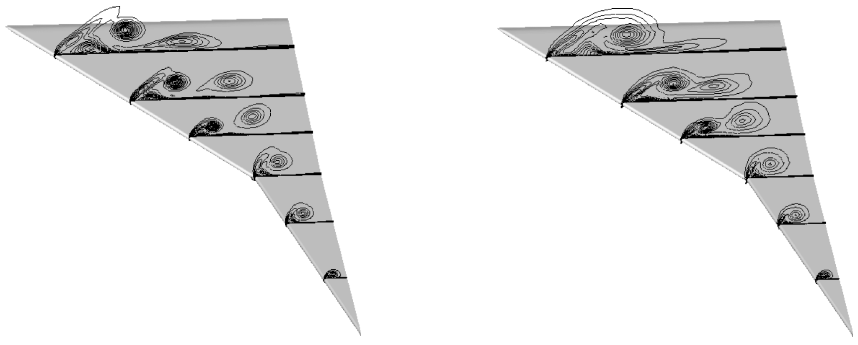

a) Compact difference scheme **b) Roe's scheme**

Fig. 5 Total pressure contour plots, $\alpha = 12$ deg and $0.86 \leq p_0/p_{0\infty} \leq 0.9975$.

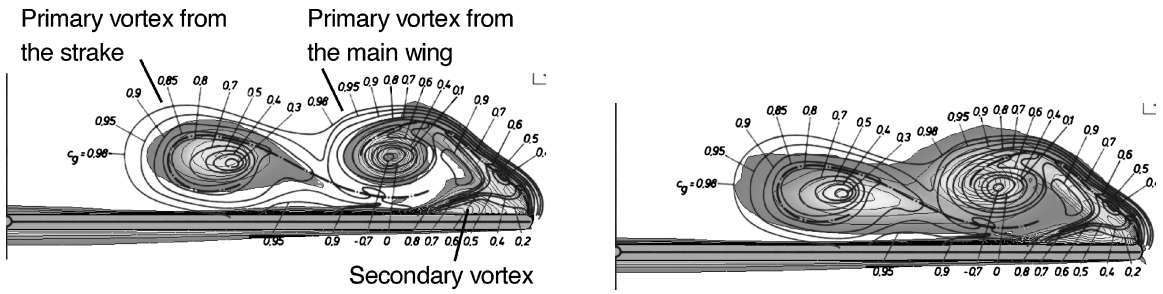

a) Compact difference scheme b) Roe's scheme

Fig. 6 Spanwise total pressure contour plots at 75% chordwise section at $\alpha = 12$ deg and $0.86 \leq p_0/p_{0\infty} \leq 0.9975$.

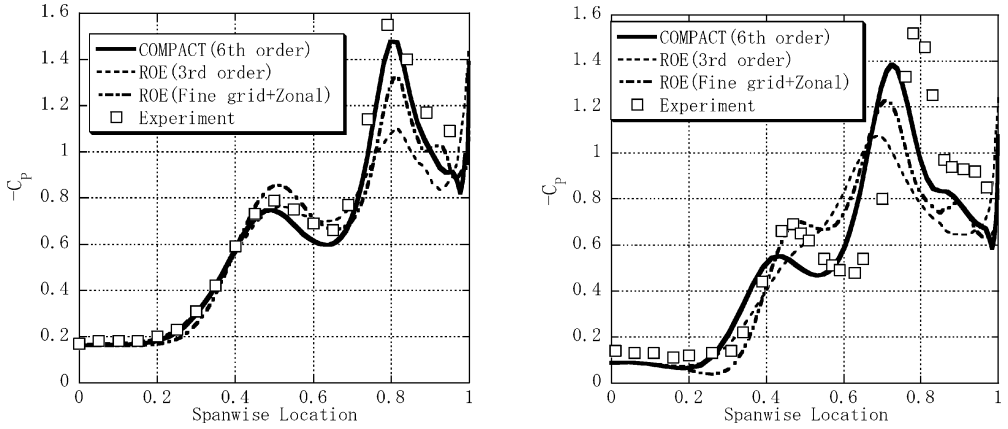

a) 62.5% chord section b) 75% chord section

Fig. 7 Spanwise C_P distributions, $\alpha = 12$ deg.

The pressure distributions on the wing surface clearly show the advantage of the compact difference scheme. Figures 7a and 7b show the pressure coefficient C_P distributions on the upper surface at the 62.5% chordwise section and the 75% chordwise section, respectively. In Figs. 7a and 7b, the results by the use of Roe's scheme on extra fine grids in our previous study[1] are plotted. In the computation indicated by "ROE (Fine grid+Zonal)," the computational grids consist of the 4 million points base grid and the 4 million points local grid near the leading edge, which is three times finer than the base grid. The fortified solution algorithm[10] is used for the interfaces between the base grid and the overset-local grid. In Figs. 7a and 7b, two negative pressure peaks are located aound 50 and 80% spanwise location with the experiment. These peaks correspond to low-pressure regions due to the vortices from the strake and the main wing. The agreement between the compact difference scheme and the experiment is excellent at the 62.5% section. It is still better than the result by Roe's scheme on 8-million grid points indicated by dot–dash line in Figs. 7. At the 75% section, the position and strength of the negative peaks disagree with the experiment in all of the simulations, but the results by use of the compact difference scheme show clear advantages against the others. The right-hand-side peak due to the vortex from the main wing is the highest among three simulations, and the second peak is clearly observed, although the position is predicted on the inner side of the wing compared with the experiment. In the result by use of Roe's scheme on the same grid, the vortices are smeared out at this section and the second peak is not captured. It is recovered by Roe's scheme on the extra fine grid, but the pressure difference between the top and the bottom is smaller than the experiment or the compact difference scheme. In summary, the sixth-order compact difference scheme is better than the Roe's third-order upwind scheme with use of 10 times more grid points. The discrepancy of the position of the second peak with the compact difference scheme is for the same reason discussed earlier (Fig. 6a), and further future investigations are necessary.

The reason for the similarity and the small differences of the aerodynamic coefficients between two schemes can be understood by the pressure distributions. The integrated areas below the curves of the pressure distributions in Figs. 7a and 7b happen to be almost the same for both results. Slightly larger pitching moments obtained by the compact scheme are due to fewer vortex interactions and the resulting pressure peaks near the trailing edge. However, the flowfields obtained by the compact difference scheme apparently show better representation of the experiment, and the rolling moments should be correctly estimated if the double-delta wing has a roll angle or a side-slip angle.

IV. Conclusions

The sixth-order compact difference scheme was applied to the flow simulation over a double-delta wing and accuracy was investigated. The scheme captured two vortices without excessive dissipations, and the secondary separation vortex near the leading edge is also properly evaluated. The resulting pressure distributions on the wing showed much better agreement with the experiment than those by use of Roe's third-order scheme. The remaining problem is the accuracy of the vortex-merging location, and further investigations are necessary to improve the reliability of the simulations.

References

[1]Horie, T., Fujii, K., and Hattori, N., "Numerical Simulations of Leading-edge Separation Vortices," *Proceedings of JSASS 15th International Sessions in 39th Aircraft Symposium*, Gifu, Japan, 2001, pp. 111–114.

[2]Brennenstuhl, U., and Hummel, D., "Vortex Formation over Double-Delta Wings," International Council of the Aeronautical Sciences, ICAS Paper 82-6.6.3, Aug. 1982.

[3]Lele, S. K., "Compact Finite Difference Scheme with Spactral-Like Resolution," *Journal of Computational Physics*, Vol. 103, No. 1, 1992, pp. 16–42.

[4]Roe, P. L., "Approximate Riemann Solvers, Parameter Vectors, and Difference Schemes," *Journal of Computational Physics*, Vol. 43, 1981, pp. 357–372.

[5]Koutsavdis, E. K., Blaisdell, G. A., and Lyrintzis, A. S., "On the Use of Compact Schemes with Partial Filtering in Computational Aeroacoustics," *AIAA Journal*, Vol. 38, No. 4, 2000, pp. 713–715.

[6]Gaitonde, D. V., and Visbal, M. R., "Further Development of a Navier–Stokes Solution Procedure Based on Higher-Order Formulas," AIAA Paper 99-0557, Jan. 1999.

[7]Visbal, M. R., and Gaitonde, D. V., "Computation of Aeroacoustic Fields on General Geometries Using Compact Difference and Filtering Schemes," AIAA Paper 99-3706, June 1999.

[8]Van Leer, B., "Toward the Ultimate Conservative Difference Scheme. 5, A Second-Order Sequel to Godunov's Method," *Journal of Computational Physics*, Vol. 32, No. 1, 1979, pp. 101–136.

[9]Fujii, K., "Efficiency Improvements of Unified Implicit Relaxation/Time Integration Algorithms and Their Applications," AIAA Paper 97-2105, June 1997.

[10]Fujii, K., "Unified Zonal Method Based on the Fortified Solution Algorithm," *Journal of Computational Physics*, Vol. 118, No. 1, 1995, pp. 92–108.

High-Order vs Low-Order Panel Methods for Unsteady Subsonic Lifting Surfaces

P. C. Chen,* Danny D. Liu,† and Darius Sarhaddi‡
ZONA Technology, Inc., Scottsdale, Arizona 85251

Introduction

THE purpose of this Note is to clarify the differences between a high-order panel method and a low-order panel method in their applications to steady and oscillating lifting surfaces in subsonic flow. The vortex lattice method is a steady low-order-lifting-surface (LOLS) method proposed by Hedman[1] and Belotserkovskii[2] during the mid-1960s. Its success led to its unsteady-flow extension, the doublet lattice method (DLM), by Albano and Rodden[3] and Rodden et al.[4,5] By "low-order" in LOLS is meant that the singularity (vortex or doublet) distribution is concentrated along the quarter-chord line on each lifting surface box. The choice of the quarter-chord location is perhaps inspired by the exact two-dimensional thin-airfoil solution or borrowed from Prandtl's lifting-line solution (but for an elliptic planform only). By the mid-1970s, Woodward[6] and PANAIR (see Ref. 7) further advanced the lifting theory, in subsonic and supersonic flow, with a fully distributed singularity over the complete box. This is defined as the high-order-lifting-surface (HOLS) method, whereby the singularity kernel is required to be integrated along chordwise and spanwise directions instead of once along the quarter-chord line as for the case of LOLS. ZONA6 (see Ref. 8) is the unsteady extension of Woodward's HOLS theory. It has long been accepted that the HOLS is an advanced version of the LOLS. LOLS, confined by its low-order nature, requires its force point (at which to evaluate pressure) to be fixed with the sending point at the quarter-chord singularity, and consequently its control point is constrained at the three-quarter-chord point in order to achieve accurate solutions. By contrast, HOLS is superior to LOLS in that its force point and control point in principle need not be prefixed, because the singularity is fully distributed. Unlike LOLS, determination of the location of these points in ZONA6 is based on countless numerical experiments for evaluation of numerous wing planforms under various flow conditions. HOLS has a sound theoretical foundation in that its formulation realizes a unified subsonic–supersonic high-order-lifting-surface method as well as a fully extended unified unsteady-flow methodology, namely, ZONA6 and ZONA7 (see Ref. 9). Lacking a sound foundation, LOLS thus far offers no unsteady supersonic counterpart, in spite of several previous attempts. In what follows, we will compare the predictions of the aerodynamic centers, the unsteady pressures, and the generalized aerodynamic forces for rectangular wings with large aspect ratios (AR) and delta wings, generated by HOLS and by LOLS.

Received 20 February 2004; revision received 1 March 2004; accepted for publication 24 March 2004.

*Vice President; pc@zonatech.com.
†President. Fellow AIAA.
‡Member of Technical Staff.

Aerodynamic Center of High-Aspect-Ratio Rectangular Wings

In Ref. 10, the author showed that the aerodynamic center (a.c.) computed by an improved DLM called N5KQ (Ref. 5) is more accurate than that computed by ZONA6 for a rectangular wing of AR 20. It is further claimed that N5KQ also predicts the a.c. at exactly the quarter-chord with one aerodynamic box along the chordwise strip, whereas ZONA6 (referred to in Ref. 1 as CPPM) predicts the a.c. at the 50% chord. This thus led the author[10] to conclude that ZONA6 is an inferior method for flutter and divergence predictions. To clarify this apparent misunderstanding in ZONA6 as a HOLS method as opposed to N5KQ as a LOLS method, we revisit the case of an AR 20 rectangular wing employed in Table 1 of Ref. 10, in which the author intended to show that N5KQ is superior to ZONA6 (with a force point assigned at the 50% chord), consistently predicting the a.c. location at 25% for all chordwise box arrangements including that due to a single box (strip). In Table 1, we show the results of ZONA6 with the force point (f.p.) assigned at the 25% chord. This time, as seen from the last a.c. column, both methods would yield nearly identical a.c. locations for almost all chordwise boxes considered. It can be seen that ZONA6 can also predict the 25% chord of the a.c. with exactly one box on the strip; as the number of boxes increases, ZONA6 predicts a slightly forward a.c. as N5KQ does. However, no exact solution exists for this case to establish which solution set is likely to be more correct.

Aerodynamic Center of Delta Wings

With the planform shape changed, the a.c. location shifts. A low-aspect-ratio wing may have an a.c. location largely different from one around the 25% chord. Here, we consider a delta wing with AR 2.31 at $M = 0.0$ whose a.c. location is obtained at 59.34% of the root chord as derived by the classical theory of Truckenbrodt.[11] Table 2 presents the a.c. locations predicted by ZONA6 (with a f.p. assigned at the 25%, 50%, and 70% chords) and by N5KQ.

As the number of boxes increases, ZONA6 with a f.p. at 70% yields an a.c. at 59.05% of the root chord, which is slightly ahead of the exact a.c. location of the 59.34% root chord. N5KQ predicts an a.c. of 58.40% of the root chord, which is ahead of the theoretical a.c. location.

The examples of Tables 1 and 2 suggest that the best f.p. location is in fact planform dependent. Confined by the LOLS formulation, the f.p. is fixed at the 25% chord for N5KQ. By contrast, ZONA6 has the freedom of assigning f.p. locations for the best a.c. solution. But as an industrial software, the f.p. location in ZONA6 should not be a user input, as it would burden the end user. With all planforms considered, we therefore select a compromise f.p. at 50% as a default value for ZONA6.

Unsteady Pressures on Delta Wings

N5KQ, as a LOLS method, is expected to yield inaccurate solutions for planforms with aerodynamic boxes of large aspect ratios. To alleviate this aspect-ratio restriction on aerodynamic box modeling, it is necessary to increase the order of the vortex-singularity distribution on the aerodynamic boxes. ZONA6, as a HOLS method, employs the constant vortex approach that results in converged solutions with high accuracy. Shown in Fig. 1 are the lifting pressure coefficients (ΔC_p) on a 70-deg delta wing at $M = 0.8$ with two types of aerodynamic box modeling: 10×10 and 40×10. In 10×10 aerodynamic box modeling, the N5KQ solutions break down at the tip strip (station 10), caused by the incompatibility of the LOLS